Entrainment rate and mixing process in a confined reverse flow reactor

Emilien Varea[a,b,*], Lukas Berger[a], Stephan Kruse[a], Heinz Pitsch[a]

[a] *Institute for Combustion Technology, RWTH Aachen University, 52056 Aachen, Germany*
[b] *CORIA UMR 6614 CNRS, INSA de Rouen, 76801 Saint Etienne du Rouvray, France*

Abstract

Moderate or Intense Low oxygen Dilution (MILD) combustion appears to be an auspicious concept to ensure low emission levels over a wide range of operating conditions. A particular geometry for the MILD combustor is provided by reverse flow reactors. In order to optimize MILD combustion, fast and efficient mixing of reactants with exhaust gases is mandatory. In this study, a reverse flow reactor is numerically set up to investigate first the flow topology – dynamic and scalar fields –, and secondly the global entrainment rate of the reverse flow to the main flow. Directly at the nozzle exit, the entrainment rate is found to be enhanced in the reverse flow configuration, resulting in a higher entrainment rate at the nozzle exit in contrast to free jets.

1. Introduction

MILD combustion [1–3], Moderate or Intense Low oxygen Dilution, appears to be an auspicious technological concept to ensure low emission levels over a wide range of operating conditions. Based on high rates of internal exhaust gas recirculation and fast dilution of fresh gases, a volumetric combustion process is achieved. The combustor can be considered as a homogeneous flow reactor where the ratio of the mixing time scale and the chemical time scale – Damköhler number – is much lower than unity. Therefore, high local temperatures are avoided, and NO_x emissions are reduced. Due to air inlet temperatures above the autoignition temperature, the process is inherently stable and because of the small and homogeneous temperature increase, there is very little combustion noise. The MILD combustion technology has already been successfully applied in furnace systems at atmospheric pressure [4]. Unlike furnace combustion processes, the conditions for MILD combustion in gas turbines are challenging. Higher pressure and temperature dramatically decrease the chemical time scale as the mixing time scale is almost unchanged. As a result, the Damköhler number increases and the process is shifted from a homogeneous flow reactor to a conventional combustion mode. To improve the process, confined reverse flow reactors have been tested and investigated [5–7]. Fuel, air and burnt gases are injected and ejected from the combustor at the same level using a concentric nozzle arrangement. The configuration presented in [6] ensures high internal recirculation of exhaust gas and dilution levels of fresh gases. However, while increasing pressure, mixing was shown to be not efficient enough [7–9] leading to still increasing pollutant emissions and decreasing efficiency. In order to stabilize MILD combustion under gas turbine conditions, fast and efficient mixing of reactants with exhaust gases is mandatory. The latter is not only a technical issue, but the lack of knowledge on turbulent mixing and mixing preparation in such flow configurations still needs to be investigated. In this study, the flow characteristics in a reverse flow reactor is investigated by performing cold flow measurement. This allows the validation of numerical simulations with experiments and therefore facilitates the evaluation of entrainment in such flow configurations. Based on numerical simulations of non-reacting flows, the aim of the project remains twofold:

- Analyze the flow topology of confined reverse flow reactors in terms of flow dynamics and scalar fields.
- Understand the mixing process and the phenomenology of entrainment between the highly turbulent main jet and the reverse flow.

2. Description of the reverse flow reactor

The reactor studied in the present work is described in detail in [8, 9]. A short description is given here. The reactor has a square cross-section with a side length of 58 mm and it is about 200 mm long. The chamber design combines a concentric arrangement of fuel and air nozzles in the exhaust exit plane of the combustor as shown in Fig. 1(a). For deflecting the gas streams, the top end of the chamber has a hemispherical shape. Since the chamber exhibits a square shape, whereas the exit and inlet planes are concentrically arranged, two investigation planes, $\theta = 0^\circ$ and $\theta = 45^\circ$, are of importance, which are indicated in Fig. 1(b). The inlet flow conditions are ambient pressure and temperature, $p = 1$ bar and $T = 300$ K, respectively. The fuel flow (8 nl/min) remains constant, while the air flow rate is adjusted to match the required equivalence ratio ϕ conditions. Two cases $\phi = 0.67$ and $\phi = 0.29$ are investigated to evaluate the mixing process, while the air to fuel ratio is

*Corresponding author:
Email address: emilien.varea@itv.rwth-aachen.de (Emilien Varea)

increased by a factor of 2.3. The injector diameter is set to $d_0 = 10$ mm, resulting in Reynolds numbers of 7200 and 16800 for $\phi = 0.67$ and $\phi = 0.29$, respectively.

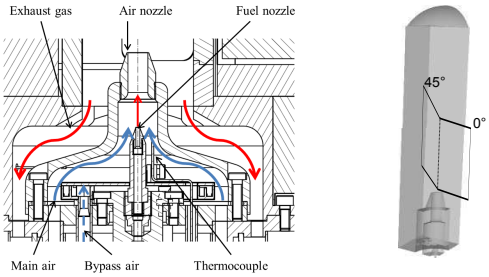

(a) Nozzle design (b) planes of interest

Figure 1: Nozzle design and investigated planes.

3. Simulation Technique

The commercial CFD software package CONVERGE^{TM} is used. CONVERGE^{TM} is a computer code for the simulation of three-dimensional, incompressible/compressible, chemically reacting transient fluid flows in complex geometries with stationary or moving surfaces. The governing equations are discretized using a finite volume scheme, and for the turbulence closure, a k-ε model is used. CONVERGE^{TM} uses a grid generation approach based on a user supplied triangulated surface. This run-time grid generation allows the grid to be changed during the simulation. The changes include scaling the cell sizes in the entire domain, locally refining or coarsening during the simulation, and adaptively refining. The adaptive mesh refinement allows for a well resolved, but still computationally efficient mesh. The refinement is based on estimating the sub-grid value of a given scalar by a Taylor series expansion, and adding refinement when a user specified threshold value for the sub-grid scalar is exceeded.

4. Results and discussion

In the following section, the topology of the fluid flow, and in particular the flow dynamics and the scalar fields, are described for the equivalence ratio $\phi = 0.67$. Afterwards, the entrainment rate for this specific jet configuration is analyzed for both flow conditions ($\phi = 0.67$ and $\phi = 0.29$).

4.1. Topology - Flow Dynamics

The fuel and air jet is injected from the air nozzle into the combustor, Fig. 1(a). Figure 2 compares results from experiments with numerical simulations, which provides a measure for the accuracy of numerical results obtained in this study. Figure 3 shows the axial velocity (simulations) in two different planes, at $\theta = 0°$ and $\theta = 45°$. Fuel and air exit velocities are about 14 and 10 m/s, respectively. For a free jet, a cone shaped opening is expected, entraining air from the environment and thus leading to a jet expansion. Since the jet is confined in the combustion chamber and due to the reverse flow configuration, a different behavior is expected. Because of the reverse flow configuration, the injected flow needs to return and depending on the total kinetic energy of the flow, stagnation points exist in a region between the point of injection and the chamber's top. Furthermore, considering the quadratic shape of the combustor, it becomes clear that the reverse flow can be found mostly in the chamber's corners, since this minimizes momentum exchange between the opposed flows. Figure 4 shows the axial velocities along different heights showing that the flow is returning in the corners to the chamber's exit.

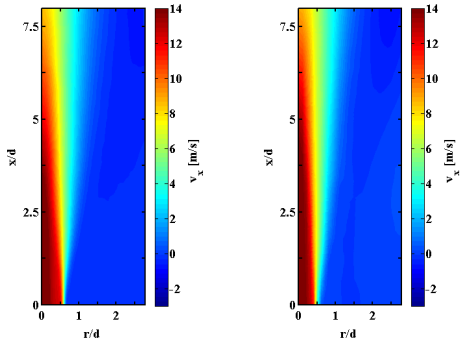

(a) Experiments (b) Simulations

Figure 2: Axial velocities at cut plane of $\theta = 0°$ from experiments (left) and simulations (right) for $\Phi = 0.67$.

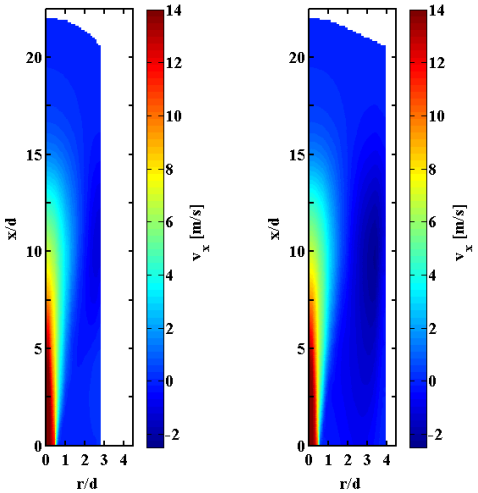

(a) $\theta = 0°$ (b) $\theta = 45°$

Figure 3: Axial velocities at cut planes of $\theta = 0°$ and $\theta = 45°$ for $\Phi = 0.67$ (simulations).

Investigating the jet's expansion process by inspecting velocity profiles along a cut plane of $\theta = 0°$ as shown in Fig. 5(a), the gas injected at the nozzle shows approximately a top hat profile form, whereas regions close to

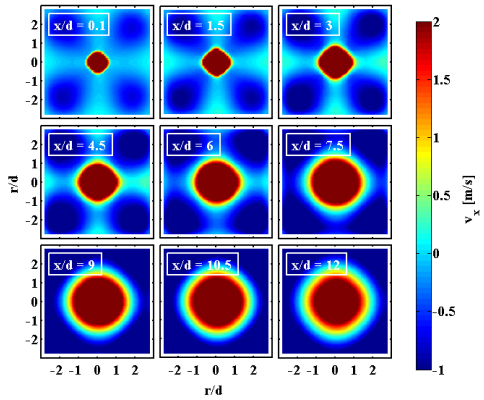

Figure 4: Axial velocities at different heights for $\Phi = 0.67$.

the nozzle wall are slowed down. For increased heights, the sharp decrease in velocity softens more and more at the jet's boundary. Thereby, the latter is defined by the point of zero axial velocity (red points in Fig. 5(a)). In the beginning, an expansion of the jet can be seen which stagnates for higher positions. From Fig. 5(b), which represents the iso-surface of zero axial velocity, the jet's boundary can be viewed in three dimensions. The combustor's corners are highlighted by regions of zero velocity at the height of 20 diameters. Furthermore, four regions of zero axial velocity are observed at the bottom part of the chamber, in the planes of $\theta = 0°$. These regions arise from the deceleration of the reverse flow due to momentum exchange with the main jet.

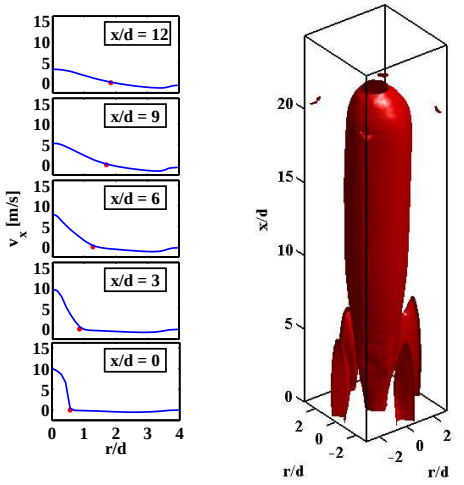

(a) Velocity profiles (b) Zero velocity isosurface

Figure 5: Axial velocity profiles at several heights (left), and zero velocity isosurface (right).

4.2. *Topology - Scalar field*

In a next step, the mixing process of fuel and air is investigated. Due to the reverse flow configuration, a shear layer develops in between the main jet and the reverse flow, and thus leading to an entrainment of gases into the jet. The shear layer can be identified as the region of increased vorticity with its maximum value close to the air nozzle as a result of the steeper velocity gradients in this region. According to Philip and Marusic [10] and Bisset et al. [11], for the turbulent mixing process, one should distinguish between i/ large scales inducing a flux from the non-vortical surrounding to the vortical central jet – engulfment, and ii/ small scales which are responsible for breaking the large scales - nibbling - and increase the turbulent degree of the induced flux. This can be seen from Fig. 6(a) showing the turbulent kinetic energy increasing from the outer to the inner part of the jet, where the mixing layer is located. According to Fig. 6(b) and Fig. 6(c) showing the mixture fraction fields, fuel and air start mixing around 8-9 diameters. In

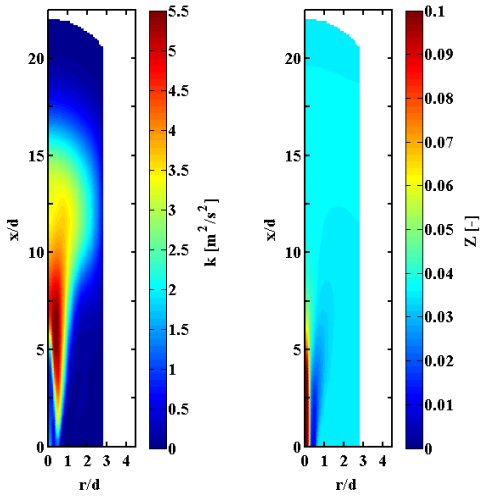

(a) Turbulent kinetic energy along the $\theta = 0°$ cut plane (b) Mixture fraction along the $\theta = 0°$ cut plane

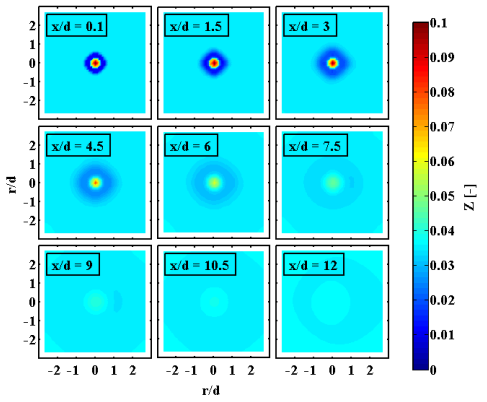

(c) Mixture fraction at different heights

Figure 6: Mixture fraction fields, cut plane along $\theta = 0°$ and horizontal cut planes for $\Phi = 0.67$.

this homogeneous case, in terms of diffusivity, viscosity and density fluid properties, mixing between fuel and air is essentially due to dynamic field fluctuations. There-

fore, it is worth noting that the mixing zone corresponds to the region of high degrees of turbulence. Meanwhile, as the mixing between fuel and air is effective, the turbulence starts decaying as shown in Fig. 7. This finally leads to the conclusion that mixing between fuel and air is a slow process, which is then intensified due to the increased degree of turbulence. At last, the decrease in turbulent kinetic energy towards the end of the combustor, shown in Fig. 6(a), is related to the smoother velocity gradients for bigger heights which was already discussed in the context of Fig. 5.

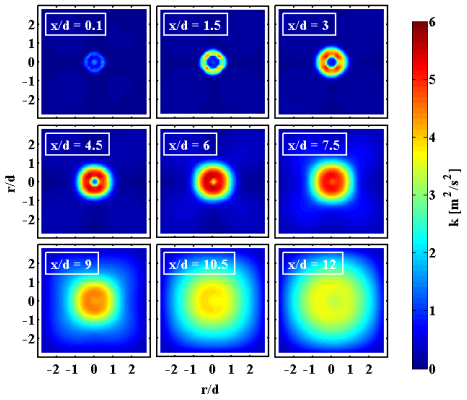

Figure 7: Turbulent kinetic energy at different heights and along $\theta = 0°$ for $\Phi = 0.67$.

4.3. *Calculating the entrainment ratio* C_e

Concerning MILD combustion, the entrained gases play a crucial role. According to Han and Mungal [12], the jet entrainment can be expressed by the recirculation ratio as

$$C_e = \frac{d^*}{\dot{m}_0} \cdot \frac{d\dot{m}}{dz} \qquad d^* = d_0 \cdot \frac{\rho_0}{\rho_\infty}, \tag{1}$$

where $\dot{m}_0$ is the inlet mass flux, $\dot{m}$ the mass flux at a given height, z the axial direction and ρ_0 and ρ_∞ are the densities inside the jet and in the far field, respectively. Hence, the C_e value describes the normalized mass growth along the height inside the jet. Han and Mungal [12] investigated free jets injected from a long tube and provide a comparison to other studies. In contrast, this jet has a reverse flow and the main jet is affected by the confinement. Moreover, the fluid is injected from a convergent nozzle instead of a long tube. Basically, there are two methods by which the entrainment rate can be determined. For a control volume as shown in Fig. 8, the entrained mass $\dot{m}_e$ can be calculated as follows:

Method A:

$$\dot{m}_{e,A} = \int_0^{R_2} (\rho \cdot v_z)|_{A_2} \cdot 2\pi r \, dr - \int_0^{R_1} (\rho \cdot v_z)|_{A_1} \cdot 2\pi r \, dr \tag{2}$$

Method B:

$$\dot{m}_{e,B} = \int_{z_1}^{z_2} (\rho \cdot v_n)|_B \cdot 2\pi \, R(z)|_B \, dz \tag{3}$$

Here terms like $(...)|_{A_1,A_2,B}$ indicate that the specific

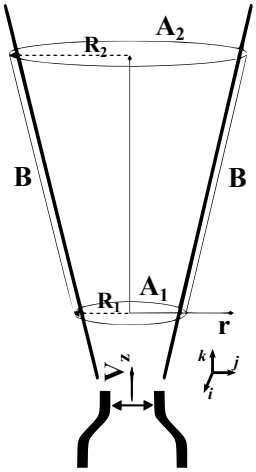

Figure 8: Scheme of the control volume.

values are evaluated along the corresponding surfaces. By continuity, it is clear that for steady state conditions, the definitions of $\dot{m}_{e,A}$ and $\dot{m}_{e,B}$ are equal. Thus, method A determines the entrainment rate by calculating the mass inside the jet at two different heights whereas the growth corresponds to the entrained mass. Method B directly computes the mass flux passing the surface B and thus the entrained mass. Accordingly, the velocity component v_n normal to the jet boundary B is needed. When placing A_1 and z_1 at the air nozzle's exit, $\dot{m}_e = \dot{m}_{e,A} = \dot{m}_{e,B}$ gives the totally entrained mass into the jet for a given height. Therefrom $d\dot{m}_e/dz$ and further the coefficient C_e can be obtained. For the calculation, $d^* = d_0$ is assumed (homogeneous flow) and $\dot{m}_0$ is considered according to

$$\dot{m}_0 = \int_0^{0.5 \cdot d_0} (\rho \cdot v_z)|_{z=0} \cdot 2\pi r \, dr \tag{4}$$

For the calculation of the entrainment rate, the numerical results are taken, since they provide three dimensional data. From PIV data an assumption of an axisymmetric jet would be necessary in order to fulfill Eq. 2 and Eq. 3.

4.3.1. *Method A*

According to Eq. 2, the jet's boundary needs to be determined in order to get R_1 and R_2. Basically, the jet's boundary is represented by the strong shear layer between the main jet and the reverse flow, which corresponds to the region of high turbulent kinetic energy and strong velocity gradients. When starting from the jet's center, the velocity decreases towards the walls and even becomes negative in the region of the returned flow. Based on these observations many definitions of the jet's

boundary are possible like the position of the highest vorticity, the highest velocity decrease, highest turbulent kinetic energy or RMS values, or taking a specific velocity value. In this case, the isosurface of zero velocity was found as the best choice for the jet's boundary. This seems reasonable in order to divide the flow into injected fluid and reverse flow. The simulations provide discrete data at the corresponding positions in the mesh. The values at the grid nodes are assumed homogeneous over the whole cells so that with respect to method A the integrals along A_1 and A_2 are approximated by sums. Thus Eq. 5 considers only grid points (i,j) inside the jet.

$$\int_0^R (\rho \cdot v_z)|_A \cdot 2\pi r \, dr \approx \sum_{i,j} \rho_{i,j} (v_z)_{i,j} \, A_{cell} \quad (\forall \, (v_z)_{i,j} \geq 0 m/s) \tag{5}$$

4.3.2. Method B

For applying method B, first the isosurface of zero axial velocity representing the jet boundary is computed. This surface is represented by a triangulation. Consequently, to calculate the mass flux entrained over the isosurface, the mass flux passing through each triangle needs to be determined. Since vertices of triangles are not necessarily identical with the grid points, the values at these vertices are interpolated from the grid data. Furthermore, to compute the mass flux, the mean velocity vector, the density and the triangle area are needed according to

$$\int_{z_1}^{z_2} (\rho \cdot v_n)|_B \cdot 2\pi \, r|_B \, dz \approx \sum_i \dot{m}_{Tr,\,i} \quad (\forall \, h_i \leq h) \tag{6}$$

$$\dot{m}_{Tr,\,i} = - \left(\rho \cdot (\vec{u} \cdot \vec{n}) \cdot A_{Tr} \right)\Big|_i \tag{7}$$

The area is determined by Eq. 8, the normal vector by Eq. 9, and the other values are calculated by the arithmetic mean of the vertices' values.

$$A_{Tr} = 1/2 \cdot (\vec{a} \times \vec{b}) \tag{8}$$

$$\vec{n} = \vec{a} \times \vec{b} / |\vec{a} \times \vec{b}| \tag{9}$$

Finally, it should be noted that for a correct calculation of the entrained mass, the normal vector needs to point from the jet into the environment. Therefore, as long as the jet expands, this requirement can be fulfilled by $n_z \leq 0$ whereas n_z indicates the normal vector's component in axial direction. Summarizing, the mass flux flowing though each triangle is determined and the whole entrained mass from the air nozzle up to a given height h can be computed by Eq. 7.

4.3.3. Analyzing the entrainment ratio

The entrainment ratio C_e is shown for both cases in Fig. 10. An entrainment ratio's resolution along the jet's axis was only possible to be determined by method A whereas method B only provides the mean C_e. It can be seen that a constant entrainment ratio is reached already after approximately 2 nozzle diameters whereas the plateau represents the linear increase of the jet's mass flux in the beginning (not shown in the paper). After a height of 8 nozzle diameters, the C_e value starts dropping whereas the values further downstream are not reliable anymore. This phenomenon can be explained by inwards pointing normals when the jet's expansion stagnates (method B), and because the fluid starts returning towards the exit, leading to decreased mass flux of the main jet (method A). Due to mass continuity, the results for the region below a height of 8 nozzle diameters seem reliable, since one would expect the same outcome for the entrainment ratios regardless of which method is applied. Thereby, calculation techniques are cross-checked, since both methods are used independently.

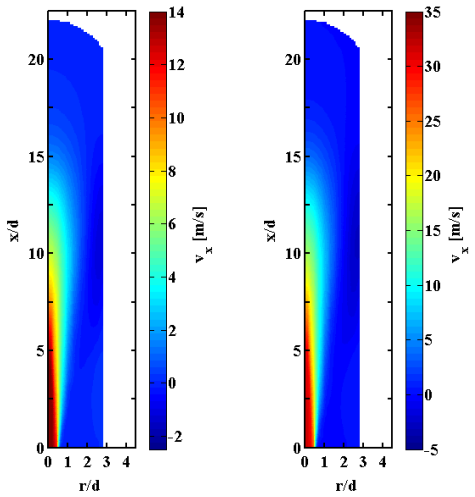

(a) $\phi = 0.67$ (b) $\phi = 0.29$

Figure 9: Axial velocities at $\theta = 0°$ for $\phi = 0.67$ and $\phi = 0.29$.

When applying method B, the plateau of a constant entrainment ratio can be found at a value of $C_e = 0,21$ for $\phi = 0.67$ and $C_e = 0,18$ for $\phi = 0.29$, respectively. Regarding the two setups, in both cases the same fuel mass flux is applied and thus resulting in much higher air mass fluxes for leaner conditions. Since the air flow is dominating the flow field, consequently much higher injection velocities appear for $\phi = 0.29$. Even though the level of velocities is different, the flow deceleration in axial direction is similar for both cases and qualitatively both jets behave similarly as shown in Fig. 9. It is not surprising that both setups have an entrainment ratio of the same magnitude, since absolute velocities remain unconsidered when determining the normalized entrainment ratio C_e.

4.3.4. Comparison to literature

The entrainment ratio of free jets has been investigated by several studies, Han and Mungal [12], Trabold et al. [13], Boguslawski and Popiel [14] and Hill [15].

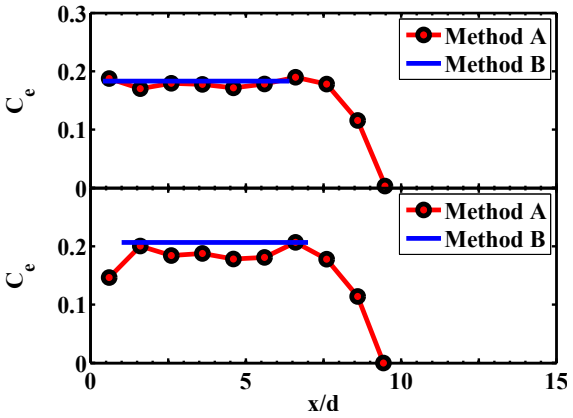

Figure 10: C_e values computed by method A and B for two equivalence ratios $\phi = 0.29$ (top) and $\phi = 0.67$ (bottom), respectively.

In Fig. 11, the results of these four studies for free jets are compared to this work dealing with a confined jet in a reverse flow configuration. According to Han and Mungal [12], the main difference among the results of Hill [15] and the other three studies is the injection jet profile. Hill [15] injects from a convergent nozzle, whereas the others use long tubes. Han and Mungal [12] conclude that jets from convergent nozzles develop faster than injected from a long tube, but eventually reach the same entrainment ratio coefficient in the far field.

In this work, a convergent nozzle is used combined to a reverse flow configuration. It seems problematic to separate the domain into a far and near field. Moreover, reliable values of the entrainment ratio could be computed only up to 8 diameters above the air nozzle as mentioned before. In contrast to free jets, the confined jet of this setup seems to be already fully developed after two nozzle diameters above the air nozzle; even the jet studied by Hill [15] needed 12 diameters to fully develop. Thus, the plateau of constant entrainment ratio is reached extremely quickly. On the other hand, the absolute value of entrainment appears to be lower than for far downstream regions of free jets.

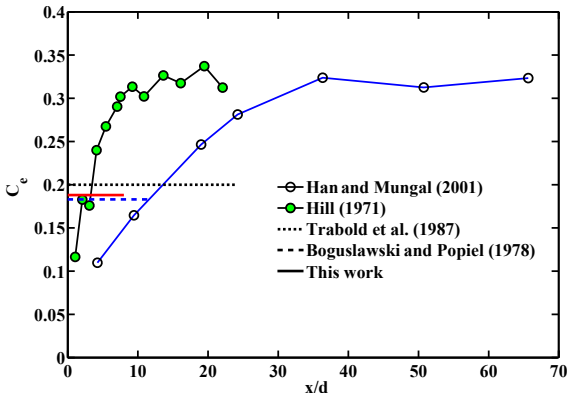

Figure 11: C_e values: Comparison to literature.

5. Conclusions

In this study, a reverse flow reactor has been successfully investigated with respect to its flow topology and entrainment behavior. Based on numerical results, the entrainment ratio C_e was found to range between 0.18 to 0.21 for both flow equivalence ratios studied ($\phi = 0.29$ and $\phi = 0.67$). Directly at the nozzle exit, the entrainment rate is found to be strongly enhanced in reverse flow combustor resulting in an established plateau regime at the nozzle exit in contrast to free jets. This clearly demonstrates that reverse flow configurations represent a good choice for MILD combustors, where fast and efficient mixing are mandatory.

References

[1] A. Cavaliere, M. Joannon, MILD combustion, Progress Energy Combust. Sci. 30 (2004) 329–366.
[2] V. Arghode, A. Gupta, Effect of flow field for colorless distributed combustion (cdc) for gas turbine combustion, Appl. Energy 87 (2010) 1631–1640.
[3] A. Khalil, A. Gupta, Swirling distributed combustion for clean energy conversion in gas turbine applications, Appl. Energy 88 (2011) 3685–3693.
[4] Y. Levy, V. Sherbaum, P. Arfi, Basic thermodynamics of FLOXCOM, the low-NO_x gas turbines adiabatic combustor, Appl. Therm. Eng. 24 (2004) 1593–1605.
[5] V. Arghode, A. Gupta, Investigation of reverse flow distributed combustion for gas turbine application, Appl. Energy 88 (2011) 1096–1104.
[6] M. Bobba, P. Gopalakrishnan, K. Periagaram, J. Seitzman, Flame structure and stabilization mechanisms in a stagnation point reverse flow combustor, J. Eng. Gat Turb. 130.
[7] S. Kruse, B. Kerschgens, L. Berger, E. Varea, H. Pitsch, Experimental and numerical study of MILD combustion for gas turbine applications, submitted to Applied Energy.
[8] S. Kruse, E. Varea, V. Wassmuth, H. Pitsch, Influence of premixing and residence time on MILD combustion in a reverse flow configuration, Proc. Combust. Inst., Poster W1P029.
[9] E. Varea, S. Kruse, T. Albin, D. Abel, H. Pitsch, Actuation studies for active control of MILD combustion for gas turbine applications, ASME Düsseldorf (2014) GT2014–27138.
[10] J. Philip, I. Marusic, Large-scale eddies and their role in entrainment in turbulent jets and wakes, Phys. Fluids 24 (2012) 055108.
[11] D. K. Bisset, J. C. R. Hunt, M. M. Rogers, The turbulent/nonturbulent interface bounding a far wake, J. Fluids Mech. 451 (2002) 383410.
[12] D. Han, M. G. Mungal, Direct measurement of entrainment in reacting / nonreacting turbulent jets, Combust. Flame 124 (2001) 370–386.
[13] T. Trabold, E. Esen, N. Obet, Entrainment by turbulent jets issuing from sharp-edged inlet round nozzles, J. Fluids Eng. 109 (1987) 248–254.
[14] L. Boguslawski, C. O. Popiel, Flow structure of the free round turbulent jet in the initial region, J. Fluid Mech. 90 (1979) 531–539.
[15] B. Hill, Measurements of local entrainment in the initial region of axisymmetric turbulent air jets, J. Fluids Mech. 51 (1972) 773779.